Research Article | Vol. 27, No. 4 | 18 Feb 2019 | OPTICS EXPRESS 5764
Optics EXPRESS

Thermal effects of ultrafast laser interaction with polypropylene

ARIFUR RAHAMAN, ARAVINDA KAR, AND XIAOMING YU*

CREOL, The College of Optics & Photonics, University of Central Florida, Orlando, FL 32816, USA
**yux@creol.ucf.edu*

Abstract: Ultrafast lasers have been used for high-precision processing of a wide range of materials, including dielectrics, semiconductors, metals and polymer composites, enabling numerous applications ranging from micromachining to photonics and life sciences. To make ultrafast laser materials processing compatible with the scale and throughput needed for industrial use, it is a common practice to run the laser at a high repetition rate and hence high average power. However, heat accumulation under such processing conditions will deteriorate the processing quality, especially for polymers, which typically have a low melting temperature. In this paper, an analytical solution to a transient, two-dimensional thermal model is developed using Duhamel's theorem and the Hankel transform. This solution is used to understand the effect of laser parameters on ultrafast laser processing of polypropylene (PP). Laser cutting experiments are carried out on PP sheets to correlate with the theoretical calculation. This study shows that, in laser cutting, the total energy absorbed in the material and the intensity are two important figures of merit to predict the cutting performance. Heat accumulation is observed at low scanning speeds and high repetition rates, leading to significant heat-affected zone and even burning of the material, which is supported by experimental data and modelling results. It is found that heat accumulation can be avoided by a proper choice of the processing condition.

1. Introduction

Ultrafast lasers have been used widely for both fundamental research and practical applications since they were developed in early 1980s [1,2]. For materials processing, ultrafast lasers offer precision, flexibility and robustness that are not easily achieved by other laser sources [3,4]. These characteristics are enabled fundamentally by the short pulse duration, high peak power, and non-thermal interaction with a wide range of materials (e.g. metals, glasses, polymers, and ceramics). Ultrafast lasers generate ultrashort pulses in the range of femtoseconds to a few tens of picoseconds, a timescale that is shorter than the thermal equilibrium time in most materials. Ultrafast lasers have been used to process varieties of materials [5–7]. Ultrafast lasers interact with different materials based on the mechanism of laser energy absorption. In semiconductors and dielectrics, laser excitation may lead to non-thermal phase transformations induced by the transient modification of interatomic bonding when a high concentration of free electrons is promoted across the bandgap [8]. In materials that have a large bandgap (such as dielectrics and some semiconductors), the excited electrons can absorb laser energy and bring the material to the plasma state or even produce the Coulomb explosion, the latter of which is due to charge separation on the surface [9]. The absorption mechanism is different for materials that are opaque, such as metals and some semiconductors at visible to near-infrared wavelengths. In these materials, linear absorption contributes the most to laser energy deposition.

The interaction of ultrashort pulses with polymeric materials has many features that make ultrashort laser systems attractive for a variety of applications. However, heat accumulation in the material at high pulse repetition rates can deteriorate the processing quality, especially for polymers which typically have a low melting temperature. The process physics to efficiently

#354954 https://doi.org/10.1364/OE.27.005764
Journal © 2019 Received 10 Dec 2018; revised 29 Jan 2019; accepted 31 Jan 2019; published 14 Feb 2019

Optics EXPRESS

cut polymeric materials with ultrafast lasers is important, especially for flexible electronics consisting of polymeric substrates. An analytical solution of the thermal model enables to calculate the temperature distributions in the substrate rapidly for various processing conditions to determine the thermal effects of different laser parameters on the material. Therefore, the analytical model can be used to select the processing parameters in various industrial applications and avoid the trial and error approach involving numerous experiments for process parameter optimization. The model will significantly reduce the time and cost of new process development, and it can be implemented to monitor and control a given process. Also, the model can provide results that are impractical to measure such as the internal temperature of the material.

Mathematical models of the thermal effects can be divided into two types: analytical and numerical models. Analytical models yield analytical solutions, representing a direct relation between laser parameters and the heating process. The analytical solutions are, however, difficult to obtain for complex systems, but can be determined under certain simplifying assumptions to gain insights into the physical processes. These solutions can be used as a guideline for optimizing the laser processing parameters. There have been several studies on analytical modeling in recent years. B.S. Yilbas *et al*. [10] introduced a one-dimensional model using the kinetic theory approach for short-pulse laser processing. Their study compared the predictions of kinetic energy theory with predictions from other models for laser pulses with pulse durations in the range of 10^{-9} to 10^{-11} s. Khenner *et al*. [11] obtained an analytical solution to the classical heat conduction problem of solid film irradiated by repetitive laser pulses using the method of separation of variables. B.S. Yilbas and Pakdemirli [12] derived a closed-form solution of the temperature distribution originated from repetitive pulsed laser heating using the perturbation method. They utilized the hyperbolic heat conduction equation derived from the Boltzman equation and its general solution, which was obtained using the Fourier transform method [13]. However, previous solutions to the hyperbolic heat conduction equation are limited in one-dimensional (1D) spatial and temporal dimensions. A. K. Nath *el. al* [14] presented a 1D model for the temperature profiles during heating and cooling cycles in repetitive pulsed laser irradiation, and the effects of processing parameters, such as laser power, beam diameter, scan speed, pulse duration, repetitive rate and duty cycle, on laser surface hardening were analyzed. Stuart *et al.* [15] developed a general theoretical model of laser interaction with dielectrics, which was shown to be in good agreement with experimental data in short pulse regime. A generalized analytical solution was presented by Tung T. Lam [16] for electron and lattice temperature profiles in a metallic film exposed to ultrashort laser pulses using the superposition and the Fourier transform method in conjunction with the solution structure theorems. Chen *et al.* [17] presented the two-dimensional analytical solutions of repetitive pulsed laser heating of aluminum alloy and investigated the effects of processing parameters on the temperature distribution. They showed that millisecond pulse duration can avoid the plasma effect. Taylor *el al* [18]. established a three-dimensional, two-temperature model (TTM) and a heat-accumulation model based on classical heat generation and conduction equations to evaluate their efficacy and efficiency in simulating non-thermal ablation and heat accumulation during multi-pulse femtosecond laser processing of silicon.

In this paper, an analytical solution to a transient, two-dimensional (2D) thermal model is developed using Duhamel's theorem and the Hankel transform for calculating the temperature distribution in polypropylene (PP) subject to femtosecond laser irradiation. The analytical solution is used to analyze the effects of processing parameters, i.e. pulse energy, scanning speed, repetition rate, focal spot size and pulse duration. Experiments are conducted on PP sheets of thickness 300 μm, which are important materials in many industrial applications, such as packaging for consumer products, plastic parts for various industries including the automotive industry, special devices like hinges, and fabrics [19], due to low cost, good flexibility, and low weight of this material. The experimental results will be used to verify the

Optics EXPRESS

model and to analyze the effects of various processing parameters. The material removal rates are found to have a linear relationship with the absorbed laser energy for different values of absorptivities under various laser-PP interaction conditions, indicating that the thermal effects of different laser parameters are similar but the optical effects, i.e., the absorptivities, are different. This study on laser-PP interactions using theoretical and experimental methods shows the feasibility of using ultrashort laser pulses to cut thin polymer materials with high precision. Also, the thermal model, which is developed in this study, can be applied to other laser materials processing applications, such as the laser heat treatment for surface hardening, laser drilling, laser ablation, and micro-and nano-structuring of surface. In addition, this model can be used to determine the temperature distribution by varying the beam shape temporally and spatially for examining the shapes and sizes of the two-dimensional and three-dimensional structures produced by a given set of laser parameters.

2. Analytical solution to a 2D transient thermal model

A 2D transient Heat Conduction Model (HCM) and its analytical solution that describe ultrashort laser pulse interaction with the workpiece is discussed in this section. The model is based on the geometry shown in Fig. 1, which depicts laser pulses irradiating on a piece of thin solid material. The workpiece is considered in an axisymmetric cylindrical coordinate system.

The absorbed laser energy is assumed to be converted to heat instantaneously. The material removal is modeled as a sublimation process where heated solid materials directly turns into vapor because the liquid phase exists only for a very short period of time [20]. For laser processing of polymeric composite materials, chemical degradation can occur before the temperature reaches the vaporization temperature [21]. For simplification, chemical degradation is treated in the same way as sublimation because both processes absorb energy and produce gases [22].

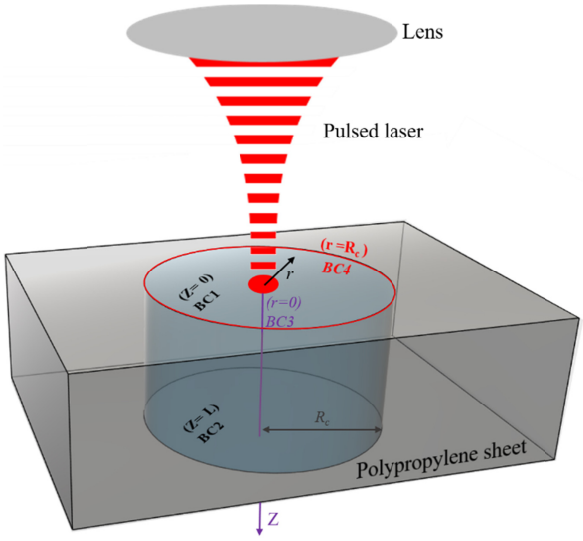

Fig. 1. Schematic of ultrashort pulse laser heating model in cylindrical coordinates with boundary conditions at four locations as BC1, BC2, BC3 and BC4 at the upper and lower surfaces, center of the cylinder and $r = R_c$, respectively.

2.1 Spatial and temporal profile of the ultrashort laser pulses

The intensity $I(r,t)$ of the Gaussian beam is given by

Optics EXPRESS

$$I(r,t) = AI_o e^{-\frac{2r^2}{\omega_o^2}} \varphi(t) \tag{1}$$

where A is the absorptivity of the workpiece; r, ω_o and $I_o = \frac{4E}{\pi\omega_o^2 t_{on}}$ are the radial coordinate, radius at the waist of the laser beam, and the peak intensity, respectively. $\varphi(t)$ is the laser pulse shape function, describing the temporal profile of the laser pulse as a function of time t. In this study $\varphi(t)$ is assumed to be a triangular shape given by

$$\varphi(t) = \begin{cases} \dfrac{t-(n_p-1)t_p}{t_{pk}} & for\ (n_p-1)t_p \le t \le (n_p-1)t_p + t_{pk} \\ \dfrac{(n_p-1)t_p + t_{on} - t}{t_{on} - t_{pk}} & for\ (n_p-1)t_p + t_{pk} < t \le (n_p-1)t_p + t_{on} \\ 0 & for\ (n_p-1)t_p + t_{on} < t \le (n_p-1)t_p + t_p \end{cases} \tag{2}$$

where $n_p = 1,2,3,4,\ldots$ are the total number of pulses irradiating on the sample, t_{on} and t_p are the laser pulse on time and period (pulse on plus pulse off time), respectively, and t_{pk} is the time at which the pulse reaches its peak intensity.

The femtosecond laser system of this study produces Gaussian pulses that were used at the pulse length of 200 fs for cutting experiments. This pulse shape can be approximated fairly well as a triangular pulse due to the high peak power and short pulse length of the Gaussian pulse. The error in the energy of a triangular pulse compared to the Gaussian pulse is 6.44% for both types of pulse having the same pulse length of 200 fs, where the Gaussian pulse length is defined as the full width at half maxima. Different pulse shapes would affect the temporal distribution of the temperature. Replacing the Gaussian pulse with a triangle pulse simplifies the thermal analysis considerably without introducing a significant error due to the small error in the pulse energy. The effects of different pulse shapes on the temperature distribution can be studied by representing the pulse shape function through the variable $\phi(t)$ in this model.

2.2 Development of the thermal model and derivation of the analytical solution

The 2D transient HCM is solved analytically in the cylindrical coordinates for a semi-infinite medium irradiated by a pulsed laser beam. As shown in Fig. 1, the origin of the coordinate system lies on the top surface of the workpiece and coincides with the center of the laser beam. The radial (r) axis is parallel to the workpiece surface and the axial (z) axis points to the bottom surface of the workpiece. Here, both r and z are considered as finite.

Considering different thermal conductivities in the r and z directions, the governing heat conduction equation is given by [23]

$$\frac{\partial^2 T(r,z,t)}{\partial r^2} + \frac{1}{r}\frac{\partial T(r,z,t)}{\partial r} + k_{zr}\frac{\partial^2 T(r,z,t)}{\partial z^2} = \frac{1}{\alpha_r}\frac{\partial T(r,z,t)}{\partial t} \tag{3}$$

Optics EXPRESS

where $k_{zr} = \frac{k_z}{k_r}$ is the ratio of thermal conductivity along z, k_z, to the thermal conductivity along r, k_r, and $\alpha_r = \frac{k_r}{\rho c_p}$ is the thermal diffusivity along the r-direction. Here, ρ and c_p are the density and specific heat of the workpiece, respectively. Since the temperature of the substrate varies during the cutting process, the temperature-dependent thermophysical properties and absorptivity affect the temperature distribution in the material as cutting progresses. Due to the paucity of high temperature data, however, thermal models are generally developed with constant values of the properties [8–10] as a first order approximation to the laser-material interaction process.

The boundary conditions (BCs) and the initial condition (IC) are

$$BC1: -k_z \left.\frac{\partial T(r,z,t)}{\partial z}\right|_{z=0} = AI(r,t). \tag{4}$$

$$BC2: -k_z \left.\frac{\partial T(r,z,t)}{\partial z}\right|_{z=L} = h\left(T_L - T_\infty\right). \tag{5}$$

$$BC3: \left.\frac{\partial T(r,z,t)}{\partial r}\right|_{r=0} = 0. \tag{6}$$

$$BC4: T\left(R_c,z,t\right) = T_\infty \tag{7}$$

$$IC: T\left(r,z,0\right) = T_o \tag{8}$$

where h is the heat transfer coefficient of the air-workpiece boundary at the lower ($z = L$) surface. Here, T_∞ and T_o are the ambient temperature and initial temperature of the workpiece, respectively, and $T_L = T(r, L, t)$ and R_c is the characteristic radius of the cylinder, which is determined in the Appendix.

To reduce the dependency of the solution on a potentially large number of dimensional parameters, dimensionless parameters are used which are defined as

$$r^* = \frac{r}{\omega_o} \qquad z^* = \frac{z}{\omega_o} \tag{9}$$

$$t^* = \frac{\alpha_r t}{\omega_o^2} \qquad T^*(r^*,z^*,t^*) = \frac{T\left(r,z,t\right) - T_\infty}{T_o - T_\infty} \tag{10}$$

where t^* is known as the Fourier number. Applying the dimensionless parameters to Eq. (3), BCs and IC, the HCM can be rewritten as

$$\frac{1}{r^*}\frac{\partial}{\partial r^*}\left(r^* \frac{\partial T^*(r^*,z^*,t^*)}{\partial r^*}\right) + k_{zr}\frac{\partial^2 T^*(r^*,z^*,t^*)}{\partial z^{*2}} = \frac{1}{\alpha_r}\frac{\partial T^*(r^*,z^*,t^*)}{\partial t^*} \tag{11}$$

which is subject to the following BCs and IC with dimensionless parameters

$$BC1: \left.\frac{\partial T^*(r^*,z^*,t^*)}{\partial z^*}\right|_{z^*=0} = -\frac{A}{k_z} I(r^*,t^*) \tag{12}$$

Optics EXPRESS

$$BC2: \left.\frac{\partial T^*(r^*,z^*,t^*)}{\partial z^*}\right|_{z^*=L^*} = -Bi\,T^*(r^*,z^*,t^*)\Big|_{z^*=L^*} \tag{13}$$

$$BC3: \left.\frac{\partial T^*(r^*,z^*,t^*)}{\partial r^*}\right|_{r^*=0} = 0 \tag{14}$$

$$BC4: T^*\left(R_c^*,z^*,t^*\right) = 0 \tag{15}$$

$$IC: T^*\left(r^*,z^*,0\right) = T_i \tag{16}$$

where $Bi = \frac{h\omega_o}{k_z}$ is Biot number, T_i = 1 and $R_c^* = \frac{R_c}{\omega_o}$. The method of solving this HCM is outlined in Appendix A to obtain the following dimensionless temperature distribution in the workpiece:

$$\begin{aligned} &T^*\left(r^*,z^*,t^*\right) \\ &= \sum_{m=1}^{\infty}\frac{J_o\left(\lambda_m^* r^*\right)}{N_H\left(\lambda_m^*\right)}\overline{\psi}_{ss}^*\left(\lambda_m^*,z^*,\tau^*\right) + \sum_{m=1}^{\infty}\frac{J_o\left(\lambda_m^* r^*\right)}{N_H\left(\lambda_m^*\right)}\sum_{n=1}^{\infty}\frac{\cos\left(\gamma_n^* z^*\right)}{N_F\left(\gamma_n^*\right)}\tilde{\tilde{T}}_t^*(\lambda_m^*,\gamma_n^*)^{e-at^*} \\ &-\sum_{m=1}^{\infty}\frac{J_o\left(\lambda_m^* r^*\right)}{N_H\left(\lambda_m^*\right)}\sum_{n=1}^{\infty}\frac{\cos\left(\gamma_n^* z^*\right)}{N_F\left(\gamma_n^*\right)}\tilde{\tilde{G}}(\lambda_m^*,\gamma_n^*)\int_0^{t^*} e^{-a(t^*-\tau)}\frac{d\varphi^*(\tau^*)}{d\tau^*}d\tau^* \end{aligned} \tag{17}$$

where the normalization constant for the Hankel transform is

$$\frac{1}{N_H(\lambda_m^*)} = \frac{2}{R^{*2}J_1^2(\lambda_m^* R^*)} \tag{18}$$

and

$$\tilde{\tilde{G}}\left(\lambda_m^*,\gamma_n^*\right) = \int_0^{L^*}\overline{\psi}_{ss}^*\,(\lambda_m^*,z^*)\cos(\gamma_n^* z^*)\,dz^* \tag{19}$$

All other variables in Eq. (3) are defined in Appendix A. Equation (3) yields the dimensional temperature distribution in terms of r, z and t as

$$T(r,z,t) = \left(T_o - T_\infty\right)T^*\left(r^*,z^*,t^*\right) + T_\infty \tag{20}$$

3. Outputs from the model

The temperature distributions in polypropylene (PP) sheets due to ultrafast laser irradiation are modeled using the above mentioned analytical solutions where the following thermophysical properties and laser parameters are used (Table 1).

Optics EXPRESS

Table 1: Thermophysical properties of PP [24–26] and laser irradiation parameters for thermal modeling

Properties and Parameters	Value
Thickness of PP workpiece, (μm)	300
Thermal decomposition temperature, T_c (K)	601
Density of the material, ρ (Kgm^{-3})	946
Thermal conductivity, k, k_r, k_z ($Wm^{-1}K^{-1}$)	0.22
Thermal diffusivity, α (m^2s^{-1})	$1.37x10^{-7}$
Specific heat capacity at constant pressure, C_p ($Jkg^{-1}K^{-1}$)	1920
Heat transfer coefficient, h (W/m^2K)	100
Pulse duration, t_{on} (fs)	200
Pulse repetition rate, N_p (MHz)	1
Pulse repetition rate, N_p (kHz)	10, 100
Laser beam radius, ω_o (μm)	18.4
Laser Wavelength, λ (nm)	1030

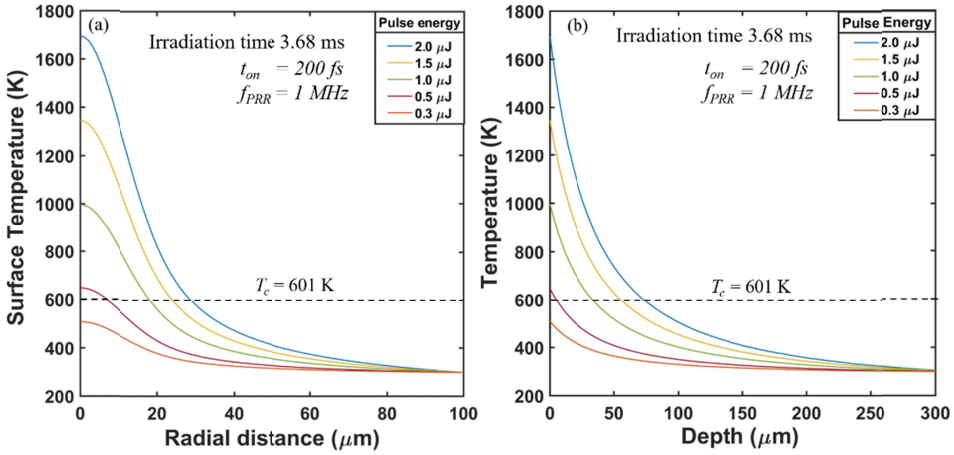

Fig. 2. Results from the thermal model for various laser parameters, (a) radially symmetric temperature distribution at the surface of the workpiece, z = 0, and (b) axial distribution of temperature at the center of the laser beam, r = 0, to examine the maximum depth of the workpiece that can be vaporized using different laser parameters.

Figure 2(a) shows the temperature distributions along the r direction at the PP surface $z = 0$ for different pulse energies from 0.3 μJ to 2 μJ. Here, the pulse repetition rate (N_p) and the pulse duration are set to 1 MHz and 200 fs, respectively. Since the laser intensity is higher at the center of the beam, the maximum temperature is reached at r = 0. In addition, higher temperature is attained for larger pulse energies because the input energy to the workpiece increases as the pulse energy is increased. The temperature distributions along the z direction at the center of the laser beam $r = 0$ is shown in Fig. 2(b) for pulse energies from 0.3 μJ to 2

Optics EXPRESS

μJ. In the model, the laser beam is absorbed at the surface (z = 0) where the highest temperature is reached for each pulse energy. The temperature decreases as the depth increases, because input energy decreases with increasing depth.

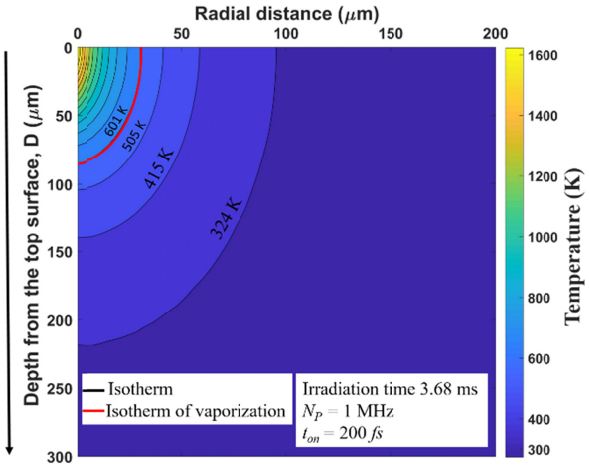

Fig. 3. 2D contour plot of temperature distribution in the workpiece, showing isotherms to indicate the removal of materials above the isotherm of vaporization temperature marked by 601 K contour.

Figure 3 shows the 2D temperature distribution in the workpiece for an average power of 2 W, repetition rate of 1 MHz and interaction time of t_i = 3.68 ms, where $t_i = \frac{2\omega_o}{v}$, where v is the laser cutting speed. The temperature at the workpiece surface (z = 0) and the laser beam center (r = 0) is around 1600 K, which is higher than the thermal decomposition temperature of PP (600 K – 700 K). By setting the temperature of 601 K (428°C) as the minimum temperature required for PP material removal, the threshold pulse energy can be determined from Fig. 3 for partial-depth cutting, D, on the upper surface or full-depth cutting, i.e., through cutting, from the upper to the lower surfaces. Similarly, the kerf width and the depth of cut for any pulse energy can be obtained from the contour graph (Fig. 3) by comparing with the known decomposition temperature of PP. The volume of the removed material can be calculated from the kerf width and the depth of cut by assuming a particular shape of the cross section such as a triangular or parabolic shape.

Figure 4(a) shows the surface temperature at the center of the laser beam as a function of time. It can be seen that the workpiece temperature increases very rapidly at the arrival of each laser pulse, which is expected because of the short pulse duration. Heat accumulation in the workpiece is higher at high pulse energies. The heat accumulation depends on the pulse energy and pulse repetition rate [27,28], which need to be optimized for efficient materials processing to avoid excessive heating and thermal damage to the material. Figure 4(b) shows the heat accumulation for the pulse energy 2 μJ at the repetition rate 1 MHz, and the laser-material interaction time 3.68 ms within which 3680 pulses are incident on the sample. It can be seen that the temperature is above the PP decomposition temperature at 0.5 ms.

Optics EXPRESS

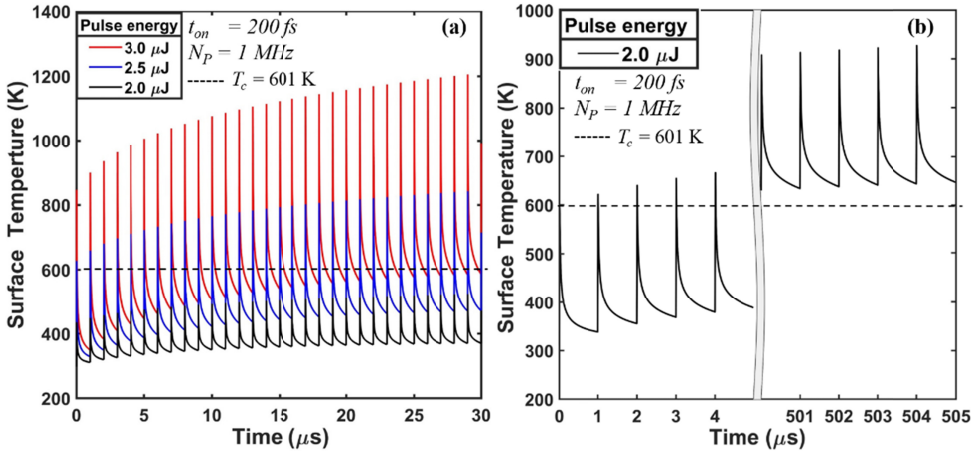

Fig. 4. Temperature distribution over time for different energies at the surface of the workpiece ($z = 0$, $r = 0$) and the decomposition temperature of PP indicated by a horizontal dash line, (a) heat accumulation with different pulses and (b) heat accumulation with 2 μJ pulse energy.

4. Experimental studies

Commercially available white PP sheets of thickness 300 μm were used in this study. The reflectance and absorption coefficient of this material are measured as 81% and 188 cm^{-1}, respectively, at the wavelength of 1030 nm. A Yb:KGW (Yb doped Potassium Gadolinium Tungstate) laser of this wavelength was used to cut the PP sheets with various laser parameters. The cross-sections of the laser cut channels were prepared using both a sharp knife and a laser beam. Since similar cross-sections were obtained by both methods, the sharp knife was used for simplicity. The sheets were placed in an upright position and the cross-sections were examined in an optical microscope to measure the width and depth of the kerf.

Figure 5 shows an experimental setup for ultrafast laser cutting of thin (300 μm) PP sheets. The laser delivers 170 fs – 10 ps laser pulses with the maximum pulse energy of 1 mJ and the repetition rate tunable up to 1 MHz. The central wavelength is 1030 nm and the maximum average output power is 6 W. The diameter of the output beam of the laser system is 4 mm which is enlarged to 10 mm by a beam expander. The laser power is controlled by an attenuator which is a variable neutral density filter. The laser beam is focused with a lens of 250 mm focal length and the workpiece is placed at the focal plane where the beam diameter is measured to be 36.8 μm at $1/e^2$-point. The surface of the workpiece is kept perpendicular to the laser beam.

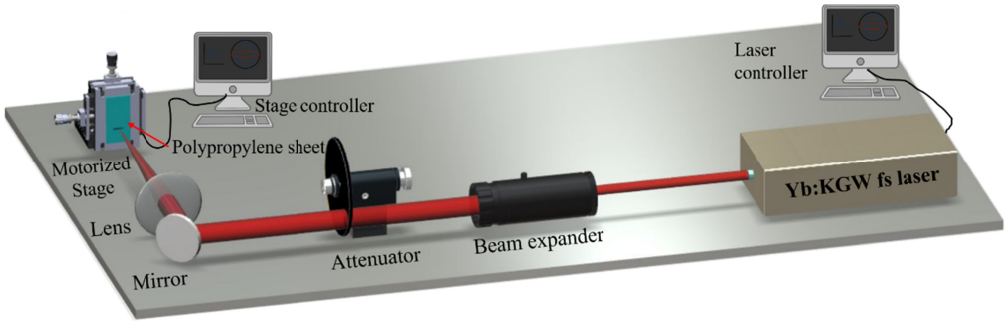

Fig. 5. Schematics of the experimental setup for laser cutting.

Optics EXPRESS

5. Results and discussion

Figure 6 shows experimental results for the effect of repetition rates on laser cutting of PP sheets at 10 mm/s. For 10 kHz repetition rate (Fig. 6(a)), each of the pulses has large pulse energy, therefore, the workpiece is heated to high temperatures resulting in a large heat-affected zone (HAZ). Figure 6(b) shows the laser cutting at 100 kHz where the overlapping area between two successive pulses is higher than that at 10 kHz. The areas of pulse overlapping on the surface of the workpiece are 96.54% and 99.65% of the area of laser spot for 10 kHz and 100 kHz, respectively, and this overlapping area is defined as $O_l = 2\omega_o^2[\cos^{-1}(\frac{v}{2\omega_o N_p}) - (\frac{v}{2\omega_o N_p})\sqrt{1-(\frac{v}{2\omega_o N_p})^2}]$. The best cutting results were observed at 100 kHz with almost no HAZ where through cuts were obtained for pulse energies > 15 µJ. Although the pulse overlapping is much higher for 100 kHz compare to previous case of Fig. 6(a), better cutting quality is obtained in Fig. 6(b) since the pulse energy is much lower than in the case of Fig. 6(a). For 1 MHz repetition rate (Fig. 6(c)), the pulse overlapping is too high (99.96%), which doesn't allow heat to dissipate in the bulk of the workpiece before the next pulse is incident on the workpiece. Therefore, the heat accumulates at the laser-material interaction zone, causing thermal damage and burning of the material as shown in Fig. 6(c). This heat accumulation effect is illustrated in Fig. 7(a).

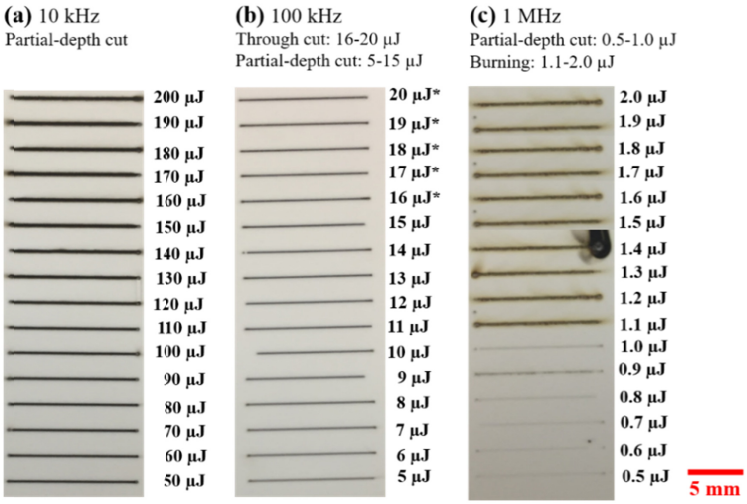

Fig. 6. Effect of different pulse repetition rates on the laser cutting process for different pulse energies with the same average powers, showing a variety of cut quality such as partial-depth cutting, through cutting and burning of the workpiece.

The upper row in Fig. 7(a) shows that the time period between two pulses is very short for 1 MHz, which doesn't allow heat to dissipate, therefore heat accumulation occurs. The lower row, on the other hand, shows longer time period between two pulses at the pulse repetition rate of 100 kHz, which provides sufficient time for heat to dissipate resulting in nearly no accumulation of heat. Figure 7(b) shows the optical microscopic top view of the workpiece after cutting experiments at 1 MHz and 100 kHz repetition rates. Partial-depth cuts were obtained for both cases, but the cuts were shallower in the case of 1 MHz pulses than for 100 kHz pulses. The reason for this effect has been explained above in Fig. 6. Significant HAZ and burning can be observed at 1 MHz and cleaner cuts can be seen at 100 kHz in Fig. 7(b). Figure 7(c) shows Scanning Electron Microscope (SEM) images for examining the cut surfaces at a higher magnification than in Fig. 7(b). These micrographs reveal wavy but cleaner kerf produced by 100 kHz pulses, whereas 1 MHz pulses produce wider kerf at the

Optics EXPRESS

surface with damaged side wall. The burning, which is observed at 1 MHz pulses, is expected to induce uncontrolled heating and vaporization of the workpiece, resulting in thermal damages and highly tapered profile of the kerf.

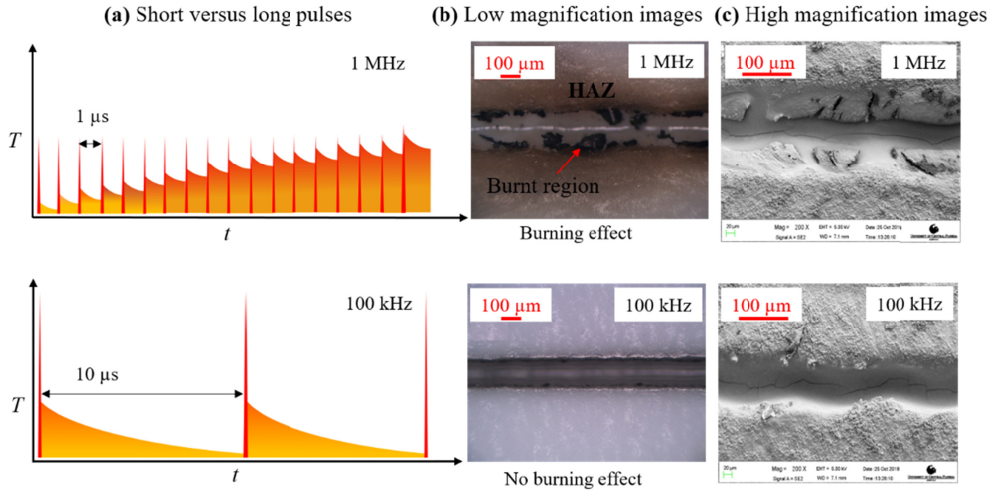

Fig. 7. Microscopic examination of the cut quality, (a) illustration of heat accumulation at a high (1 MHz) repetition rate, (b) optical microscopic images of laser cut PP sheets at 1 MHz and 100 kHz with the same average power 1.5 W and (c) SEM images of the sheets in (b) for analyzing the cut quality at a higher magnification.

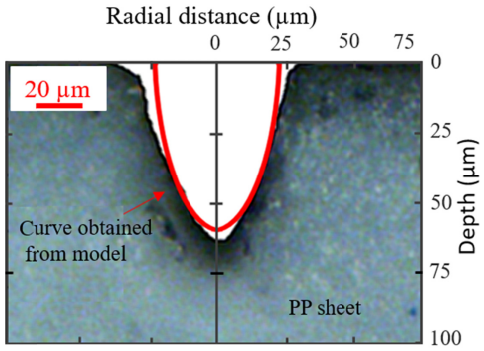

Fig. 8. Comparison between the experimental kerf profile and the model result obtained at the cutting speed of 20 mm/s with a laser of pulse energy 20 µJ and 100 kHz repetition rate.

Figure 8 shows the cross-sectional view of a laser cut channel in PP. This partial-depth cutting was accomplished with 20 µJ pulse energy and 100 kHz repetition rate at 20 mm/s cutting speed. Figure 8 also shows a theoretical cross-section determined from the 2D thermal model corresponding to the isotherm of the decomposition temperature (601 K) of PP. The shapes of different isotherms are discussed in Fig. 3. It can be seen that the experimental and theoretical results match fairly well. The discrepancies between the two profiles may be due to the variations in the thermophysical properties and absorptivity of PP at high temperatures during laser cutting.

Optics EXPRESS

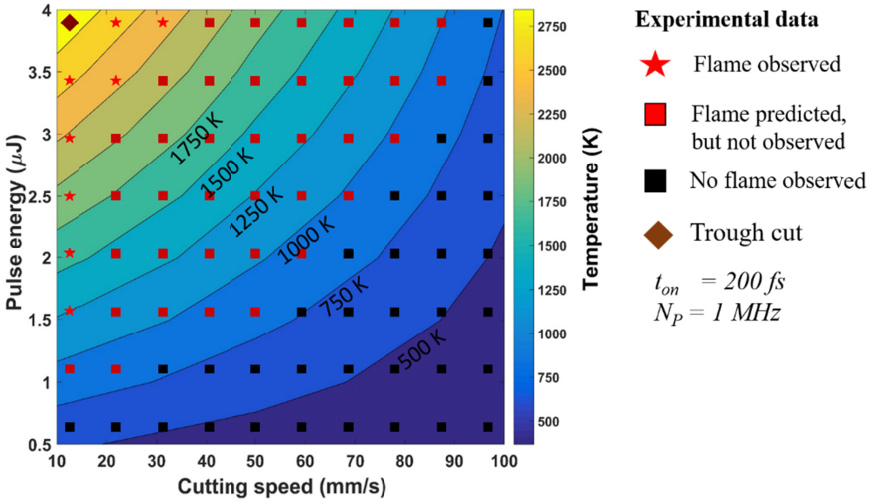

Fig. 9. A process parameter map containing theoretical isotherms and experimental results to delineate different physical effects such as through cut and burning observed during the interaction between the ultrafast laser and PP workpiece.

During the experiments, burnings of PP, i.e. flames, were observed for low cutting speeds (10 mm/s) at high pulse repetition rates (1 MHz). Burning is caused by the self-ignition of the material when the temperature exceeds a threshold temperature of self-ignition which is > 850 K for PP [29]. Figure 9 represents a laser-material interaction map based on experimental data and the thermal model to predict the occurrence of burning. The effects of four different experimental conditions are analyzed in Fig. 9. The experimental data show that PP self-ignites at a low cutting speed (10 mm/s) around a temperature of 1150 K. No burning is observed at higher cutting speeds and higher pulse energies (e.g., 60 mm/s and 4 μJ). The model, however, predicts the occurrence of burning under these conditions since the thermal energy carried away by the vaporized material is neglected in the model. It is postulated that when the cutting speed is high, more materials are expelled from the laser-material interaction zone and they remove a large amount of the energy deposited by the laser on the workpiece. Therefore, the temperature never reaches the self-ignition temperature.

During the cutting process, the polymeric material undergoes various phase changes, including thermal degradation, chemical decomposition of the atomic bonds in the polymeric chains, polymer vapor, and a plasma plume consisting of both positive and negative ions and neutral elements. The absorption of laser energy will, therefore, change during the cutting process, and this effect can be included in the model by considering temperature-dependent or time-dependent absorptivity. It should be noted that the thermophysical properties of the substrate, i.e., the thermal conductivity, density and specific heat capacity, are also temperature-dependent. These properties including the absorptivity are, however, considered constant in this study to simplify the thermal analysis of the ultrashort pulse cutting process.

The absorptivity is assumed to be 20% to obtain all of the above-mentioned results from the thermal model. However, the absorptivity is expected to vary with temperature depending on various cutting conditions. This effect is examined in Fig. 10, showing that different values of absorptivity can be estimated for different cutting conditions by comparing the experimental cut depths with the model prediction for the depth of heating. The theoretical temperature distribution yields a critical depth at which the temperature is just the decomposition temperature (601 K) of PP, and higher temperature occurs at lower depths. Therefore, the kerf will form due to material removal up to the critical depth. The temperature distribution is determined by varying the absorptivity in the mathematical model to match the critical depth with the experimental cut depth as shown in Fig. 10.

Optics EXPRESS

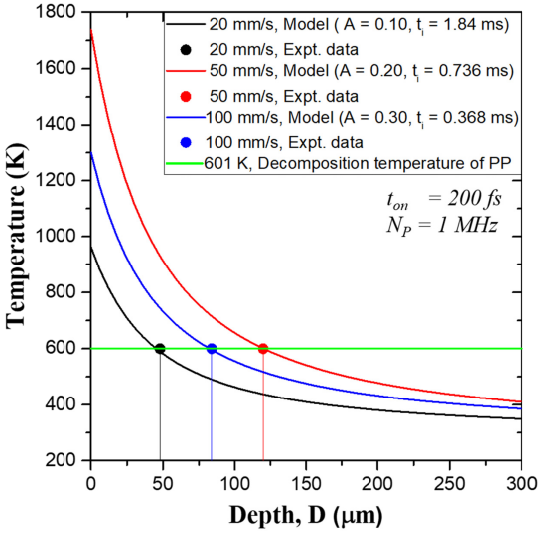

Fig. 10. Estimation of absorptivity by fitting the theoretical results to experimental data on partial cut depths at r = 0 for different cutting speeds.

The absorptivities are estimated as 0.1, 0.2 and 0.3 for 20 mm/s, 50 mm/s and 100 mm/s, respectively, at 1 MHz repetition rate. The optical properties of PP are expected to vary with the laser processing conditions since vapor and possibly plasma plume is generated at high pulse repetition rates and low cutting speeds. The vapor and plasma plume can reflect and absorb the laser energy as the beam passes through these media and, therefore, reduce the amount of laser energy reaching the surface of the material [30]. This effect is modeled by lowering the absorptivity so that a lesser amount of the incident laser energy is deposited as heat in the workpiece.

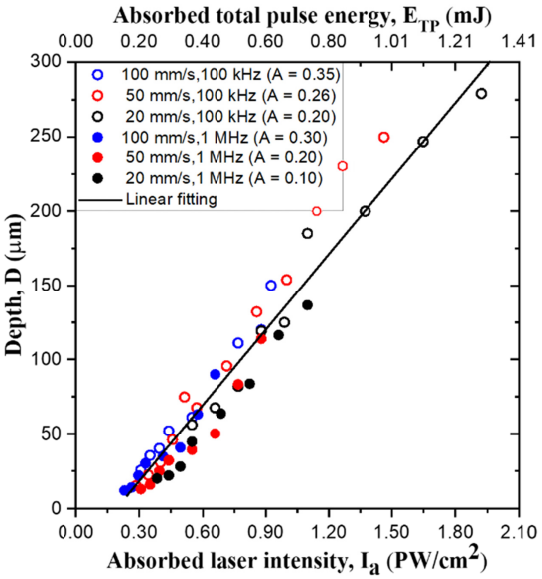

Fig. 11. Experimental data for the depth of cavity formed during laser cutting at different speeds and repetition rates, showing that the cut depths follow the same trend as a function of absorbed intensity.

Optics EXPRESS

Experiments were performed to examine the effects of various processing parameters such as the repetition rate, scanning speed, pulse energy and the laser beam diameter. Figure 11 shows the depth of cut as a function of the "absorbed total pulse energy" (upper *x*-scale), $E_{TP} = \frac{2\omega_o A E_p N_p}{v}$ and the "absorbed laser intensity [31]" (lower *x*-scale), $I_a = \frac{2AE_pN_p}{\omega_o v t_{on}}$ .The depth of the cavity formed by the removed material coincides to a single straight line in Fig. 11 for different values of absorptivity under various laser-PP interaction conditions, indicating that the thermal effects of different laser parameters are similar but the optical effects, i.e., the optical response of the material to the laser parameters, are different. The absorptivities for different processing conditions can be estimated by comparing the results of HCM with the experimental results of the cavity depth as explained in Fig. 10. The experimental data are fitted as the following linear equation

$$D = b(I_a - I_{a_o}) \tag{21}$$

where the slope, b, and the threshold absorbed intensity for material removal, I_{a_o}, are found to be 0.0178 cm^3/PW and 0.21 PW/cm^2, respectively. Using this linear relationship, one can estimate the "total energy or total intensity" to cut any thickness of PP sheet.

To study the effect of the absorbed power on the volume of material removed during the cutting process, an Overall Energy Model (OEM) is presented by considering an energy balance between the total amount of absorbed laser energy and the heat losses due to conduction in the workpiece and the heating of the vaporized material as discussed in Appendix B. The heat loss, H_l, occurs due to conduction through the two side walls of the kerf, and the heating energy loss, H_e, occurs due to the heating of the removed material from room temperature to the vaporization temperature. This model yields by following equation:

$$v w_k D = \frac{1}{H_e}\left(AE_pN_p\right) - \frac{H_l}{H_e} \tag{22}$$

where w_k is the kerf width produced during partial-depth cutting of the workpiece. Here, H_e and H_l are the heating energy and the heat energy loss, respectively, as discussed in Appendix B.

Figure 12 compares this linear relationship, Eq. (22), with experimental results and yields the heating energy H_e = 1.28 J/mm^3 as the slope of the straight line and the heat energy loss H_l = 0.263 W as the intercept of the straight line on the x-axis at which D = 0. Therefore, H_l can be interpreted as the threshold absorbed laser power for material removal, i.e., $H_l = (AE_pN_P)_o$, and Eq. (22) can be rewritten as $v w_k D = \frac{\left(AE_pN_p\right) - (AE_pN_p)_o}{H_e}$. Two significant unknown parameters in Eq. (22) are the absorptivity A and the final temperature T_f besides the thermophysical properties of the material. T_f and A can be estimated using the HCM as discussed in Fig. 10. The values of T_f, which were determined for different pulse energies 1 to 4 μJ, vary from 612 to 1555 K for 20 mm/s, 717 to 1974 K for 50 mm/s, and 629 to 1625 K for 100 mm/s cutting speeds. While the HCM provides a detailed analysis of the thermal energy distribution by the heat conduction mechanism during laser heating, the OEM yields a simple linear equation to analyze experimental data for determining the energy loss due to conduction and the utilization of energy for vaporization.

Optics EXPRESS

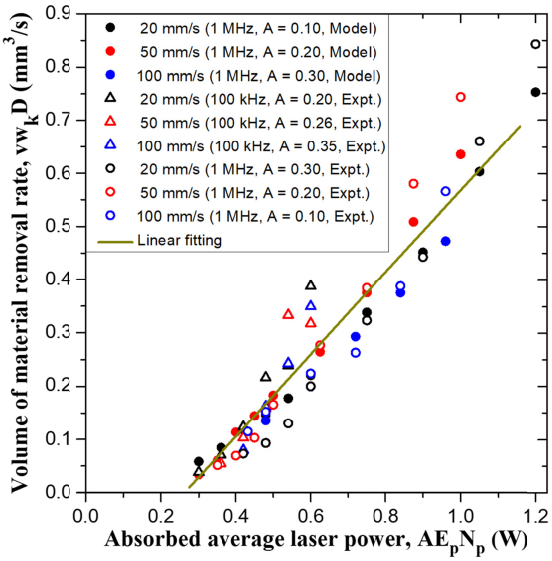

Fig. 12. Comparison between the experimental data for the material removal rate as a function of absorbed average power during laser cutting and the corresponding linear trend predicted by an overall energy balance model.

6. Conclusions

An analytical solution to the governing equation for heat transfer in ultrashort laser pulse heating of solid PP sheets is obtained using the integral transform method and Duhamel's theorem. The temperature distributions for radial and axial locations are modeled, and the effects of repetition rate and scanning speed are investigated. The calculation using the model and the measured the depth of cut and kerf width are in good agreement. From experimental studies, it is observed that a repetition rate of 100 kHz is capable of producing clean, through cut at pulse energies of tens of μJ. The depths of cavities under partial-depth cutting conditions with different laser parameters collapse into a single straight line as a function of intensity. A simple overall energy balance model is presented, showing that the volumes of vaporized material also coincide on a single straight line as a function of the absorbed laser power. Experimental data can be analyzed using this overall energy model to determine the conduction loss of energy and the utilization of energy for vaporizing the removed material.

Acknowledgments

The authors thank Dr. Xinpeng Du, Boyang Zhou and He Cheng for their helpful discussion. The authors also thank Yingjie Chai for his support in SEM imaging.

Appendix A: Solution of Heat Conduction Model (HCM):

Eq. (11) is transformed to Eq. (23) by applying the zeroth order Hankel integral transform for finite media $\overline{T}^*\left(\lambda_m^*,z^*,t^*\right)=\int_0^{R_c^*} r^* J_o\left(\lambda_m^* r^*\right)T^*(r^*,z^*,t^*)dr^*$, where λ_m^* is the m-th eigenvalue, m = 1,2,3, …, corresponding to the radial boundary conditions and J_o is the Bessel function of the first kind of zeroth order. The integral transform also yields an eigenvalue expression, $J_o\left(\lambda_m^* R_c^*\right)=0$, which is used to determine m-number of values of λ_m^*

$$k_{zr}\frac{d^2\overline{T}^*(\lambda_m^*,z^*,t^*)}{dz^{*2}}-\lambda_m^{*2}\overline{T}^*\left(\lambda_m^*,z^*,t^*\right)=\frac{d\overline{T}^*(\lambda_m^*,z^*,t^*)}{dt^*} \qquad (23)$$

Optics EXPRESS

which must satisfy the following BCs and IC

$$BC1: \left.\frac{d\overline{T}^{*}(\lambda_m^{*},z^{*},t^{*})}{dz^{*}}\right|_{z^{*}=0} = -\frac{A}{k_z}\overline{I}(\lambda_m^{*},t^{*}) \tag{24}$$

$$BC2: \left.\frac{d\overline{T}^{*}(\lambda_m^{*},z^{*},t^{*})}{dz^{*}}\right|_{z^{*}=L^{*}} = -Bi\,\overline{T}^{*}\left(\lambda_m^{*},z^{*},t^{*}\right)\Big|_{z^{*}=L^{*}} \tag{25}$$

$$IC: \overline{T}^{*}\left(\lambda_m^{*},z^{*},0\right) = \overline{T}_i(\lambda_m^{*}) \tag{26}$$

The Hankel transformed laser intensity $\overline{I}(\lambda_m^{*},t^{*})$ and initial condition $\overline{T}_i(\lambda_m^{*})$ are given by the following expressions:

$$\overline{I}\left(\lambda_m^{*},t^{*}\right) = \int_0^{R_c^{*}} r^{*} J_o\left(\lambda_m^{*} r^{*}\right) I(r^{*},t^{*})\,dr^{*} \tag{27}$$

$$\overline{T}_i\left(\lambda_m^{*}\right) = \int_0^{R_c^{*}} r^{*} J_o\left(\lambda_m^{*} r^{*}\right) T_i\; dr^{*} \tag{28}$$

The integral in Eq. (27) has a closed form result $\frac{I_o\varphi(t^{*})}{4}e^{-\frac{\lambda_m^{*2}}{8}}$ when $R_c^{*}\to\infty$. To utilize this closed form expression in the HCM for obtaining an analytical temperature distribution, the integral in Eq. (27) is evaluated numerically for sufficiently large values of R_c^{*} and different values of λ_m^{*} so that the numerical value of the integral matches well with the result of the closed form expression. This approach yielded $R_c^{*} =$ 10.5 and therefore R_c = 193.2 μm, which indicates that the PP sheet can be considered radially infinite for radii larger than or equal to 10 times the laser beam radius, i.e., $R_c = 10.5\omega_0$.

Using Duhamel's theorem on Eq. (23), the new governing equation can be rewritten as

$$k_{zr}\frac{d^2\overline{\psi}^{*}(\lambda_m^{*},z^{*},t^{*},\tau^{*})}{dz^{*2}} - \lambda_m^{*2}\overline{\psi}^{*}\left(\lambda_m^{*},z^{*},t^{*},\tau^{*}\right) = \frac{d\overline{\psi}^{*}(\lambda_m^{*},z^{*},t^{*},\tau^{*})}{dt^{*}} \tag{29}$$

and the boundary and initial conditions, (A2), (A3) and (A4), can be expressed as

$$BC1: \left.\frac{d\overline{\psi}^{*}(\lambda_m^{*},z^{*},t^{*},\tau^{*})}{dz^{*}}\right|_{z^{*}=0} = -\frac{A}{k_z}\overline{I}(\lambda_m^{*},\tau^{*}) \tag{30}$$

$$BC2: \left.\frac{d\overline{\psi}^{*}(\lambda_m^{*},z^{*},t^{*},\tau^{*})}{dz^{*}}\right|_{z^{*}=L^{*}} = -Bi\,\overline{\psi}^{*}\left(\lambda_m^{*},z^{*},t^{*},\tau^{*}\right)\Big|_{z^{*}=L^{*}} \tag{31}$$

$$IC: \overline{\psi}^{*}\left(\lambda_m^{*},z^{*},0,\tau^{*}\right) = \overline{T}_i(\lambda_m^{*}) \tag{32}$$

The solution to Eq. (29), $\overline{\psi}^{*}\left(\lambda_m^{*},z^{*},t^{*},\tau^{*}\right)$, can be split into the following transient and steady state solutions:

Optics EXPRESS

$$\overline{\psi}^{*}\left(\lambda_m^{*},z^{*},t^{*},\tau^{*}\right)=\overline{\psi}_H^{*}\left(\lambda_m^{*},z^{*},t^{*}\right)+\overline{\psi}_{ss}^{*}\left(\lambda_m^{*},z^{*},\tau^{*}\right) \tag{33}$$

The governing equation for the transient solution can be obtained from Eqs. (29) and (33):

$$k_{zr}\frac{d^2\overline{\psi}_H^{*}(\lambda_m^{*},z^{*},t^{*})}{dz^{*2}}-\lambda_m^{*2}\overline{\psi}_H^{*}(\lambda_m^{*},z^{*},t^{*})=\frac{d\overline{\psi}_H^{*}(\lambda_m^{*},z^{*},t^{*})}{dt^{*}} \tag{A12}$$

and the boundary and initial conditions for Eq. (34) is determined from Eqs. (33), (30), (31) and (32):

$$\left.\frac{d\overline{\psi}_H^{*}\left(\lambda_m^{*},z^{*},t^{*}\right)}{dz^{*}}\right|_{z^{*}=0}=0 \tag{35}$$

$$\left.\frac{d\overline{\psi}_H^{*}(\lambda_m^{*},z^{*},t^{*})}{dz^{*}}\right|_{z^{*}=L^{*}}+Bi\,\overline{\psi}_H^{*}\left(\lambda_m^{*},z^{*},t^{*}\right)\Big|_{z^{*}=L^{*}}=0 \tag{36}$$

$$\overline{\psi}_H^{*}\left(\lambda_m^{*},z^{*},0\right)=\overline{T}_i\left(\lambda_m^{*}\right)-\overline{\psi}_{ss}^{*}(\lambda_m^{*},z^{*},\tau^{*}) \tag{37}$$

Similarly, Eqs. (29) and (33) yield the following governing equation for the steady state solution:

$$\frac{d^2\overline{\psi}_{ss}^{*}(\lambda_m^{*},z^{*},\tau^{*})}{dz^{*2}}-\frac{\lambda_m^{*2}}{k_{zr}}\overline{\psi}_{ss}^{*}\left(\lambda_m^{*},z^{*},\tau^{*}\right)=0 \tag{38}$$

with the boundary conditions determined from Eqs. (33), (30) and (31) as

$$\left.\frac{d\overline{\psi}_{ss}^{*}\left(\lambda_m^{*},z^{*},\tau^{*}\right)}{dz^{*}}\right|_{z^{*}=0}=\overline{I}(\lambda_m^{*},\tau^{*}) \tag{39}$$

$$\left.\frac{d\overline{\psi}_{ss}^{*}(\lambda_m^{*},z^{*},\tau^{*})}{dz^{*}}\right|_{z^{*}=L^{*}}+Bi\,\overline{\psi}_{ss}^{*}\left(\lambda_m^{*},z^{*},\tau^{*}\right)\Big|_{z^{*}=L^{*}}=0 \tag{40}$$

The solution of Eq. (37) can be written as

$$\overline{\psi}_{ss}^{*}\left(\lambda_m^{*},z^{*},\tau^{*}\right)=C_3\left[-\left\{\frac{Bi\sinh\left(\frac{\lambda_m^{*}}{\sqrt{k_{zr}}}L^{*}\right)+\frac{\lambda_m^{*}}{\sqrt{k_{zr}}}\cosh\left(\frac{\lambda_m^{*}}{\sqrt{k_{zr}}}L^{*}\right)}{\frac{\lambda_m^{*}}{\sqrt{k_{zr}}}\sinh\left(\frac{\lambda_m^{*}}{\sqrt{k_{zr}}}L^{*}\right)+Bi\cosh\left(\frac{\lambda_m^{*}}{\sqrt{k_{zr}}}L^{*}\right)}\right\}\cosh\left(\frac{\lambda_m^{*}}{\sqrt{k_{zr}}}z^{*}\right)+\sinh\left(\frac{\lambda_m^{*}}{\sqrt{k_{zr}}}z^{*}\right)\right] \tag{41}$$

where $C_3=-\dfrac{A\sqrt{k_{zr}}}{k_z\lambda_m^{*}}\overline{I}\left(\lambda_m^{*},\tau^{*}\right)$.

Eq. (34) is solved by applying the Fourier integral transform

$$\overline{\overline{\psi}}_H^{*}\left(\lambda_m^{*},\gamma_n^{*},t^{*}\right)=\int_0^{L^{*}}\cos(\gamma_n^{*}z^{*})\,\overline{\psi}_H^{*}(\lambda_m^{*},z^{*},t^{*})dz^{*} \tag{42}$$

Optics EXPRESS

where $\cos(\gamma_n^* z^*)$ is the eigenfunction with γ_n^* as the n-th eigenvalue for n = 1,2,3,…, corresponding to the axial boundary conditions. The eigenvalues γ_n^* are determined from the transcendental equation $\gamma_n^* tan\left(\gamma_n^* L^*\right) = Bi$.

Eq. (34) simplifies to the following first order ordinary differential equation under the Fourier transform (A20):

$$\frac{d\overline{\overline{\psi}}_H^*\left(\lambda_m^*, \gamma_n^*, t^*\right)}{dt^*} + \left(k_{zr}\gamma_n^{*2} + \lambda_m^{*2}\right)\overline{\overline{\psi}}_H^*\left(\lambda_m^*, \gamma_n^*, t^*\right) = 0 \tag{43}$$

and the initial condition (A15) transforms to the following expression:

$$\overline{\overline{\psi}}_H^*\left(\lambda_m^*, \gamma_n^*, 0\right) = \overline{\overline{T}}_i\left(\lambda_m^*\right) - \overline{\overline{\psi}}_{ss}^*(\lambda_m^*, \gamma_n^*, \tau^*) \tag{44}$$

Under this initial condition (A22), the solution to Eq. (43) is

$$\overline{\overline{\psi}}_H^*\left(\lambda_m^*,, \gamma_n^*, t^*\right) = \overline{\overline{\psi}}_H^*\left(\lambda_m^*,, \gamma_n^*, 0\right) e^{-\left(k_{zr}\gamma_n^{*2} + \lambda_m^{*2}\right)t^*} \tag{45}$$

Applying the inverse Fourier integral transform to Eq. (45) and using Eq. (33), the solution to Eq. (29) can be written as

$$\begin{aligned}\overline{\psi}^*\left(\lambda_m^*, z^*, t^*, \tau^*\right) = \sum_{n=1}^{\infty} \frac{\cos(\gamma_n^* z^*)}{N_F\left(\gamma_n^*\right)} \left[\overline{\overline{T}}_i\left(\lambda_m^*, \gamma_n^*\right) - \overline{\overline{\psi}}_{ss}^*\left(\lambda_m^*, \gamma_n^*, \tau^*\right)\right] e^{-\left(k_{zr}\gamma_n^{*2} + \lambda_m^{*2}\right)t^*} \\ + \overline{\psi}_{ss}^*\left(\lambda_m^*, z^*, \tau^*\right)\end{aligned} \tag{46}$$

where the normalization constant, $N_F\left(\gamma_n^*\right)$, for the Fourier transform is given by

$$\frac{1}{N_F(\gamma_n^*)} = \frac{2\left(\gamma_n^{*2} + Bi^2\right)}{L^*\left(\gamma_n^{*2} + Bi^2\right) + Bi} \tag{47}$$

and $\overline{\overline{T}}_i\left(\lambda_m^*, \gamma_n^*\right) = \int_0^{L^*} \overline{T}_i\left(\lambda_m^*\right) \cos(\gamma_n^* z^*)\, dz^*$.

Duhamel's theorem relates the solution $\overline{\psi}^*\left(\lambda_m^*, z^*, t^*, \tau^*\right)$ to the solution $\overline{T}^*(\lambda_m^*, z^*, t^*)$ of the original problem in Eq. (A1) by the following integral

$$\overline{T}^*\left(\lambda_m^*, z^*, t^*\right) = \int_0^{t^*} \frac{\partial \overline{\psi}^*\left(\lambda_m^*, z^*, t^*, \tau^*\right)}{\partial t^*} d\tau^* \tag{48}$$

which yields the Hankel transformed temperature distribution as

$$\begin{aligned}\overline{T}^*\left(\lambda_m^*, z^*, t^*\right) = \overline{\psi}_{ss}^*\left(\lambda_m^*, z^*, \tau^*\right) + \sum_{n=1}^{\infty} \frac{\cos(\gamma_n^* z^*)}{N_F\left(\gamma_n^*\right)} \overline{\overline{T}}_i\left(\lambda_m^*, \gamma_n^*\right) e^{-at^*} \\ - \sum_{n=1}^{\infty} \frac{\cos(\gamma_n^* z^*)}{N_F\left(\gamma_n^*\right)} \left[\overline{\overline{\psi}}_{ss}^*\left(\lambda_m^*, z^*, 0\right) e^{-at^*} - \int_0^{t^*} e^{-a(t^* - \tau^*)} \frac{d}{d\tau^*}\left\{\overline{\psi}_{ss}^*\left(\lambda_m^*, \gamma_n^*, \tau^*\right)\right\} d\tau^*\right]\end{aligned} \tag{49}$$

Optics EXPRESS

where $a = \left(k_{zr}\gamma_n^{*2} + \lambda_m^{*2}\right)$. The inverse Hankel transform of this expression yields the temperature distribution $T^*\left(r^*, z^*, t^*\right)$ as given in Eq. (17).

Appendix B: Derivation of the Overall Energy Model (OEM)

Eq. (22) is derived by considering an overall energy balance per unit time for the absorbed laser energy, loss of energy due to heat conduction in the substrate and the amount of energy used for heating the removed material from room temperature to a final temperature T_f so that T_f is higher than the vaporization temperature of the material. The quasi-steady state energy balance over a time t is written as

$$N_p E_p At = \frac{1}{2} v w_k D \rho \left[c_p \left(T_m - T_o\right) + H_m + H_v + c_p \left(T_f - T_m\right) \right] t + k \frac{\left(T_f - T_o\right)}{\sqrt{\alpha t_{on}}} v t_{on}^2 N_p d_p t + k \frac{\left(T_f - T_o\right)}{2\sqrt{\alpha t_{off}}} v (t_{on} + t_{off}) d_p t_{off} N_p t \quad (50)$$

where the first term on the left-hand side is the absorbed laser energy. The first term on the right-hand side is the total amount of energy required to heat a volume of material to produce the kerf. The kerf profile is considered to have a triangular shape of width w_k and depth D. The second and third terms are the heat losses through the two side walls of the kerf due to conduction during the pulse-on and pulse-off times respectively. Since the temperature of the side walls decreases rapidly during the pulse-off time, an average temperature $(T_f + T_o)/2$ is considered to estimate the conduction heat loss due to a linear thermal gradient over a thermal boundary layer of width $2\sqrt{\alpha t_{off}}$, where α is the thermal diffusivity. Also, the conduction heat loss occurs during the pulse-off time over the side wall length of vt_{on} produced during the pulse-on time and the length of vt_{off} created during the pulse-off time, which appears in Eq. (50) as $v(t_{on} + t_{off})$.

In Eq. (50), $d_p = \frac{vD}{2N_p\omega_o}$, T_f, T_m and k are the kerf depth created per pulse, the final temperature reached during the cutting process, the melting temperature and thermal conductivity of the material, respectively. The other variables H_m, H_v, and t_{off} represent the latent heats of melting and vaporization, and the pulse-off time, respectively. H_m and H_v are irrelevant for the case of ablating PP [22].

Eq. (50) can be simplified to Eq. (22) with the following expressions for H_e and H_l:

$$H_e = \frac{1}{2}\rho \left[c_P \left(T_f - T_o\right) + H_m + H_v\right]; \quad (51)$$

$$H_l = \sqrt{k\rho c_P}\,\frac{\left(T_f - T_o\right)}{4}\,\frac{v^2 D}{\omega_o}\left[2t_{on}^{3/2} + t_{off}^{3/2} + t_{on}\sqrt{t_{off}}\right] \quad (52)$$

References

1. W. Sibbett, A. A. Lagatsky, and C. T. A. Brown, "The development and application of femtosecond laser systems," Opt. Express **20**(7), 6989–7001 (2012).
2. K. Sugioka and Y. Cheng, "Ultrafast Lasers – reliable tools for advanced material processing," Light Sci. Appl. **3**(4), e149 (2014).
3. R. R. Gattass and E. Mazur, "Femtosecond laser micromaching in transparent materials," Nat. Photonics **2**(4), 219–225 (2008).
4. S. Mishra and V. Yadava, "Laser Beam Micro-Machining (LBMM) – A review," Opt. Lasers Eng. **73**, 89–122 (2015).
5. K. C. Phillips, H. H. Gandhi, E. Mazur, and S. K. Sundaram, "Ultrafast laser processing of materials: a review," Adv. Opt. Photonics **7**(4), 684–712 (2015).

Optics EXPRESS

6. M. Malinauskas, A. Žukauskas, S. Hasegawa, Y. Hayasaki, V. Mizeikis, R. Buividas, and S. Juodkazis, "Ultrafast laser processing of materials: from science to industry," Light Sci. Appl. **5**(8), e16133 (2016).
7. S. Nolte, M. Will, J. Burghoff, and A. Tünnermann, "Ultrafast laser processing: New options for three-dimensional photonic structures," J. Mod. Opt. **51**(16-18), 2533–2542 (2004).
8. M. Hase, P. Fons, K. Mitrofanov, A. V. Kolobov, and J. Tominaga, "Femtosecond structural transformation of phase-change materials far from equilibrium monitored by coherent phonons," Nat. Commun. **6**(1), 8367 (2015).
9. N. M. Bulgakova, R. Stoian, A. Rosenfeld, I. V. Hertel, and E. E. B. Campbell, "Electronic transport and consequences for material removal in ultrafast pulsed laser ablation of materials," Phys. Rev. B Condens. Matter Mater. Phys. **69**(5), 054102 (2004).
10. B. S. Yilbas and S. Z. Shuja, "Laser short-pulse heating of surfaces," J. Phys. D Appl. Phys. **32**(16), 1947–1954 (1999).
11. M. Khenner and V. K. Henner, "Temperature of spatially modulated surface of solid film heated by repetitive laser pulses," J. Phys. D Appl. Phys. **38**(23), 4196–4201 (2005).
12. B. S. Yilbas and M. Pakdemirli, "Analytical solution for temperature field in electron and lattice sub-systems during heating of solid film," Physica B **382**(1-2), 213–219 (2006).
13. B. S. Yilbas, A. Y. Al-Dweik, and S. Bin Mansour, "Analytical solution of hyperbolic heat conduction equation in relation to laser short-pulse heating," Physica B **406**(8), 1550–1555 (2011).
14. A. K. Nath, A. Gupta, and F. Benny, "Theoretical and experimental study on laser surface hardening by repetitive laser pulses," Surf. Coat. Tech. **206**(8–9), 2602–2615 (2012).
15. B. C. Stuart, M. D. Feit, S. Herman, A. M. Rubenchik, B. W. Shore, and M. D. Perry, "Optical ablation by high-power short - pulse lasers," J. Opt. Soc. Am. B **13**(2), 459–468 (1996).
16. T. T. Lam, "A generalized heat conduction solution for ultrafast laser heating in metallic films," Int. J. Heat Mass Tran. **73**, 330–339 (2014).
17. G. Chen, Y. Wang, J. Zhang, and J. Bi, "An analytical solution for two-dimensional modeling of repetitive long pulse laser heating material," Int. J. Heat Mass Tran. **104**, 503–509 (2017).
18. L. L. Taylor, R. E. Scott, and J. Qiao, "Integrating two-temperature and classical heat accumulation models to predict femtosecond laser processing of silicon," Opt. Mater. Express **8**(3), 648–658 (2018).
19. H. A. Maddah, "Polypropylene as a promising plastic: A Review," Am. J. Pol. Sci. **6**(1), 1–11 (2016).
20. V. I. Mazhukin, I. Smurov, C. Surry, and G. Flamant, "Overheated metastable states in polymer sublimation by laser radiation," Appl. Surf. Sci. **86**(1-4), 7–12 (1995).
21. Y. K. Godovsky, *Thermophysical properties of Polymers*, (Springer, 1992).
22. C. Zang, I. A. Salman, N. R. Quick, and A. Kar, "Two-dimensional transient modeling of CO2 laser drilling of microvias in high density flip chip substrates," in ICALEO (LIA, 2005), pp. 404–411.
23. M. N. Özişik and D. W. Hahn, *Heat conduction*, (Wiley, 2010).
24. C. Maier and T. Calafut, *Polypropylene: The Definitive User's Guide and data book*, (Elsevier, 2008).
25. S. J. Kalita, S. Bose, H. L. Hosick, and A. Bandyopadhyay, "Development of controlled porosity polymer-ceramic composite scaffolds via fused deposition modeling," Mater. Sci. Eng. C **23**(5), 611–620 (2003).
26. S. Zhang and A. R. Horrocks, "A review of flame retardant polypropylene fibres," Prog. Polym. Sci. **28**(11), 1517–1538 (2003).
27. S. Eaton, H. Zhang, P. Herman, F. Yoshino, L. Shah, J. Bovatsek, and A. Arai, "Heat accumulation effects in femtosecond laser-written waveguides with variable repetition rate," Opt. Express **13**(12), 4708–4716 (2005).
28. F. Bauer, A. Michalowski, T. Kiedrowski, and S. Nolte, "Heat accumulation in ultra-short pulsed scanning laser ablation of metals," Opt. Express **23**(2), 1035–1043 (2015).
29. R. Anandjiwala, L. Hunter, R. Kozlowski, and G. Zaikov, *Textiles for sustainable development*, (Nova Science Publishes, 2007), Chap. 19.
30. A. Kar, J. A. Rothenflue, and W. P. Latham, "Scaling laws for thick-section cutting with a chemical oxygen-iodine laser," J. Laser Appl. **9**(6), 279–286 (1997).
31. A. Kar and J. Mazumder, "Two-dimensional model for material damage due to melting and vaporization during laser irradiation," J. Appl. Phys. **68**(8), 3884–3891 (1990).